Spatiotemporal Structures of Edge Limit-Cycle Oscillation before L-to-H Transition in the JFT-2M Tokamak

T. Kobayashi,[1,*] K. Itoh,[2,3] T. Ido,[2] K. Kamiya,[4] S.-I. Itoh,[3,5] Y. Miura,[4] Y. Nagashima,[3,5] A. Fujisawa,[3,5] S. Inagaki,[3,5] K. Ida,[2,3] and K. Hoshino[4]

[1]*Interdisciplinary Graduate School of Engineering Sciences, Kyushu University, Kasuga 816-8580, Japan*
[2]*National Institute for Fusion Science, Toki 509-5292, Japan*
[3]*Itoh Research Center for Plasma Turbulence, Kyushu University, Kasuga 816-8580, Japan*
[4]*Japan Atomic Energy Agency, Naka 311-0193, Japan*
[5]*Research Institute for Applied Mechanics, Kyushu University, Kasuga 816-8580, Japan*

(Received 26 March 2013; published 17 July 2013)

In this Letter, we report analyses of spatiotemporal dynamics of turbulence and structure in the limit-cycle oscillation (LCO) that precedes an L-to-H transition. Zonal flows are not observed during LCO, and the oscillation is the periodic generations or decays of barrier with edge-localized mean flow. Oscillatory Reynolds stress is found to be too small to accelerate the LCO flow, by considering the dielectric constant in magnetized toroidal plasmas. Propagation of changes of the density gradient and turbulence amplitude into the core is also observed.

DOI: 10.1103/PhysRevLett.111.035002 PACS numbers: 52.25.Fi, 52.35.Ra, 52.55.Fa

The dynamical evolution of turbulence and transport in structural transitions in magnetically confined plasmas, such as the transition to the H mode [1], is the key to understanding the turbulent transport of plasmas in a laboratory and the Universe. The physics of the H mode has been developed based on the fundamental role of radial electric field (E_r) in the transition and the suppression of turbulence [2,3]. In order to study the nonlinear mechanism associated with the H-mode transition, studies have been made on the limit-cycle oscillation (LCO) near a transition boundary in parameter space. Fundamental mechanisms of the edge-localized modes in a dithering H mode [4], i.e., the LCO among mean E_r and transport, was explained [5]. Studies of the zonal flow [6] have developed, and another type of limit cycle among zonal flow and turbulence was proposed [7]. Recently, measurements on the evolution of turbulence intensity and E_r in the LCO were made [8–13]. Many of these discussed the hypothesis that the turbulence drives zonal flows, which later suppress the turbulence. However, the assessment of the causality between turbulence and flow is sometimes controversial on the same device [14,15], E_r is often deduced from indirect measurement, and the identification of zonal flows in LCO has not yet been completed.

In this Letter, we report the analysis of spatiotemporal dynamics of turbulence and structure in the LCO at the frequency of ~4.5 kHz that precedes the L-to-H-mode transition on the JFT-2M tokamak. The electric potential is directly measured by the multiple-point heavy ion beam probes (HIBP) [16]. In this case, zonal flows are not observed during the LCO, and the oscillation is the periodic generations or decays of moderate transport barrier with localized E_r near the edge (~1 cm inside from surface). The Reynolds stress is found to be much smaller than what is necessary for the acceleration of the flow in the LCO. Propagation of changes of the density gradient and turbulence amplitude into the core is also observed, which can be related with the fast change of core transport at the onset of the H-mode transition [17].

JFT-2M is a medium size tokamak with a major radius (R) of 1.3 m and an averaged minor radius (a) of 0.3 m. The experiments were conducted with the neutral beam injection with the power of 750 kW in the codirection, the toroidal magnetic field (B_t) of 1.17 or 1.28 T, the plasma current (I_p) of 190 kA, and an upper single-null divertor configuration where the ∇B drift of an ion is directed toward the X point. The safety factor at the flux surface enclosing 95% of the total poloidal flux q_{95} was 2.9, and the line averaged electron density was 1.1×10^{19} m^{-3} before the L-H transition (see Ref. [16] for details).

The HIBP on JFT-2M gives the electrostatic potential ϕ and the HIBP secondary beam intensity I_{HIBP} at four sample volumes (6 mm × 2 mm) simultaneously, with a sampling time of 1 μs. The positions of sample volumes are as follows [16,18]. (i) For parameters of beam energy $W_0 = 350$ keV and $B_t = 1.28$ T, they are aligned on the same magnetic surface at $r - a \sim -1.0 \pm 0.5$ cm and give the poloidal wave number. (ii) For $W_0 = 350$ keV and $B_t = 1.17$ T, the angle between the row of the sample volumes and the normal vector of the magnetic surface is $\alpha \sim \pi/3$. This allows us to measure radial structures. By moving the radial position of observation in configuration (ii), while the radial distance between neighboring channels is almost fixed to ~0.25 cm, the edge region (-5 cm $< r - a < 0$ cm) is measured in a shot-by-shot manner. In addition, the continuous radial scan of the sample volumes (-10 cm $< r - a < 0$ cm) with a frequency of 500 Hz is also used to check the observations in the shot-by-shot scan.

Figure 1 shows time evolution of D_α emission intensity and electrostatic potential ϕ at $-1.25\ \mathrm{cm} < r - a < -0.25\ \mathrm{cm}$ and their wavelet power spectrum density. The L-to-H transition occurs at $t \sim 0.735$ s in this discharge (shown by the solid black line). High frequency fluctuations (>40 kHz) are observed and are suppressed at the onset of transition. The geodesic acoustic mode oscillations (GAM, at $f_{\mathrm{GAM}} \sim 15$ kHz [18]) are observed until 15 ms before the transition. Intensive and bursty LCO are observed at a frequency of $f_{\mathrm{LCO}} \sim 4.5$ kHz (HWHM $\sim$ 1.0 kHz) both in D_α and ϕ signals from $t \sim 0.722$ s. The LCO is routinely observed in this series of experiments. However, their duration time and amplitude differ shot by shot, and the peak time for the LCO amplitude does not show correlation with the onset time of the L-to-H transition. Mirnov coils (near the vacuum vessel) show a coherent magnetic perturbation at $f \sim 6$ kHz in the L mode. Only a weak correlation is seen between the magnetic and HIBP signals at $f \sim 6$ kHz. We thus focus on the analysis of signals from HIBP and D_α. In this Letter, we denote the high frequency oscillation ($f > 40$ kHz), the LCO dynamics ($f \sim 4.5$ kHz), and gradual change of parameters ($f < 2$ kHz) by such notations as, e.g., $\tilde{\phi}$, $\hat{\phi}$, and $\bar{\phi}$ for the electrostatic potential, respectively. The time averaged amplitudes of the oscillations are shown as $|\tilde{\phi}|$ or $|\hat{\phi}|$.

During the LCO period, a mean electric field in the range of $-2\ \mathrm{kV/m} < \bar{E}_r < 0\ \mathrm{kV/m}$ is observed (the radial profile of which is shown later). The $E \times B$ velocity is in the range of $0\ \mathrm{m/s} < \bar{V}_{E\times B} < 1700\ \mathrm{m/s}$ in the electron diamagnetic direction. The profile of ion temperature T_i is measured with the charge exchange spectroscopy, and the electron temperature T_e is assumed to be the same as T_i, according to Ref. [19]. In the edge region ($r - a = -1$ cm), $T_i \sim T_e \sim 130 \pm 30$ eV is observed, and the electron diamagnetic velocity is given as $V_{d,e} = T_e/(eB_t L_n) \sim 4000 \pm 1000$ m/s, where L_n is the gradient length of the electron density profile.

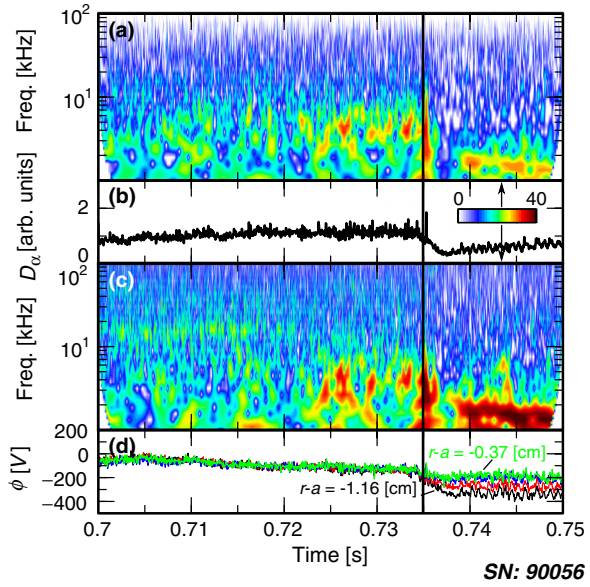

FIG. 1 (color online). Typical time evolutions of (a) normalized wavelet power spectrum density and (b) raw signal of D_α emission intensity on the divertor. Time evolutions of (c) normalized wavelet power spectrum density and (d) raw signals of electrostatic potential evaluated at four HIBP sample volumes, where the signal at the most inner location is used to calculate (c). Contours (a) and (c) are drawn in units of dB.

The high frequency fluctuations ($f > 40$ kHz) are analyzed. The procedure of the analysis is explained in Ref. [18], and the result is as follows. The poloidal mode number is estimated as $m \sim -20$ (i.e., $k_\theta \sim -0.7 \pm 0.1\ \mathrm{cm}^{-1}$) for $f \sim 50$ kHz. The absolute value of phase velocity is larger than the mean $E \times B$ velocity. That means the phase of the waves propagates in the electron diamagnetic drift direction in the laboratory and plasma frames. The wave number along the row of the sample volumes for configuration (ii) k_{path} is measured. The radial wave number is deduced as $k_r = (k_{\mathrm{path}} - k_\theta \sin\alpha)/\cos\alpha \sim -1 \pm 0.5\ \mathrm{cm}^{-1}$, at the inside of the plasma surface $r - a < -1$ cm. Fluctuations are preferentially propagating inward. The relative change of signal intensity I_{HIBP}, which indicates that of electron density n_e when the beam attenuation is ineffective $\tilde{\mathcal{N}} \equiv \tilde{I}_{\mathrm{HIBP}}/\bar{I}_{\mathrm{HIBP}}$, $\tilde{\phi}$, and the phase difference between $\tilde{\mathcal{N}}$ and $\tilde{\phi}$ is analyzed. It is found that $|\tilde{\mathcal{N}}| \sim 0.033$ and $e|\tilde{\phi}|/T_i \sim 0.045 \pm 0.01$ at $r - a \sim -1$ cm, where the key phenomena in the LCO occur. The phase difference between them is $\sim 0.4\pi$. These indicate the relation $\tilde{\mathcal{N}} \sim e^{-i0.4\pi} e\tilde{\phi}/T_e$. Therefore, the high frequency fluctuations are considered to be drift wave turbulence.

The poloidal mode number of ϕ in the LCO is found to be $m = 0$. The radial structure of the LCO dynamics in the domain of $-5\ \mathrm{cm} < r - a < 0$ cm can be given by analyzing the correlation of fluctuating quantities (from a series of discharges) with the coherent LCO modulation in D_α emission. The radial profiles of amplitude and relative phase [with respect to $\hat{D}_\alpha(t)$] in the LCO are summarized in Fig. 2. The time averages of these are taken over the time window, in which the amplitude of $\hat{D}_\alpha(t)$ exceeds a threshold value. The dependence on the choice of this threshold value is found weak. Each calculated amplitude is normalized by a factor $|\hat{D}_{\alpha,\mathrm{ref}}|/|\hat{D}_\alpha|$, where the reference value $|\hat{D}_{\alpha,\mathrm{ref}}|$ is chosen as $|\hat{D}_\alpha|$ of the discharge 90 048. This reduces the influence of imperfect reproducibility among discharges, although not completely. Figures 2(a)–2(d) show the LCO amplitudes of $\hat{\phi}$, $\hat{E}_r$, $\hat{\mathcal{N}}$, and $\hat{\mathcal{S}}/\bar{\mathcal{S}}$, where the fluctuation amplitude $\mathcal{S}(t)$ is defined as $\mathcal{S} = (\tilde{\phi}^2 + H[\tilde{\phi}]^2)^{1/2}$ and $H[\ldots]$ indicates the Hilbert transform. The cross coherence with respect to $\hat{D}_\alpha$ is also shown by the background hatched pattern in Figs. 2(a)–2(d). Figures 2(e)–2(h) show the cross

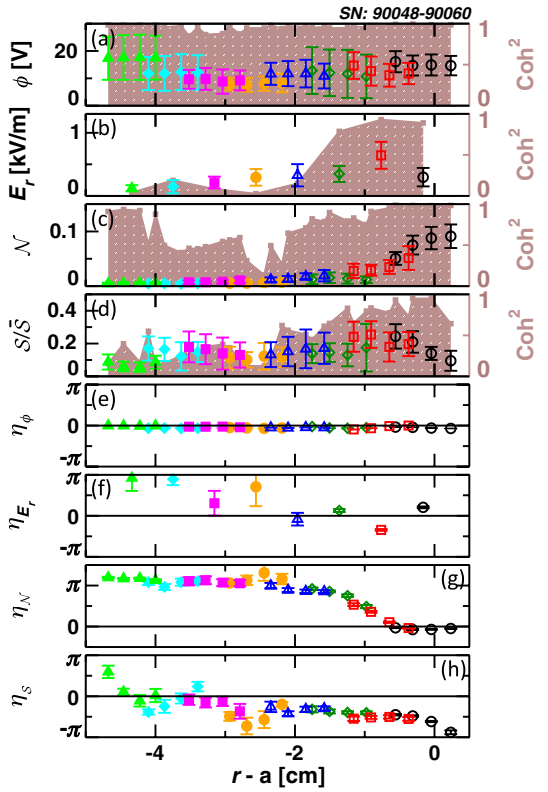

FIG. 2 (color online). Radial profiles of LCO amplitude and cross coherence with respect to D_α for (a) ϕ, (b) E_r, (c) $\mathcal{N}$, and (d) $\mathcal{S}/\bar{\mathcal{S}}$. Radial profiles of phase difference on LCO frequency between D_α intensity and (e) ϕ, (f) E_r, (g) $\mathcal{N}$, and (h) $\mathcal{S}$. Error bars represent statistical deviation.

phase η between $\hat{D}_\alpha$ and $\hat{\phi}$, $\hat{E}_r$, $\hat{\mathcal{N}}$, and $\hat{\mathcal{S}}$, where a positive value indicates the phase delay of the signal of interest with respect to $\hat{D}_\alpha$. The LCO in ϕ has almost constant amplitude with high cross coherence ~ 1. There is no radial dependence of η_ϕ, i.e., $k_r \sim 0$. This means that the LCO in ϕ is obviously *not* zonal flow, contrary to conjectures in a couple of studies (e.g., Refs. [8,11]). The radially constant part of $\hat{\phi}$ is due to a change of plasma surface potential. The electric field fluctuation $\hat{E}_r$ is evaluated by a difference of ϕ at two HIBP channels (radial distance is ~ 7 mm). In outer locations $r - a > -2$ cm, high cross coherence of E_r is observed, showing that the LCO in E_r exists only at the outer radii. The peak amplitude $|\hat{E}_r| \sim 600$ V/m is observed around the pivot point of $r - a \sim -1$ cm, with a corresponding modulation in $E \times B$ flow of ~ 500 m/s. The LCO amplitude of $\hat{\mathcal{N}}$ is large in the edge region $r - a > -1$ cm. The phase $\eta_\mathcal{N}$ has a "pivot point" at $r - a \sim -1$ cm, across which the LCO phase jumps by the amount of π. This phase inversion implies the periodic increment or reduction of the density gradient, i.e., generation or decay of a transport barrier. The modulation of turbulence amplitudes $\hat{\mathcal{S}}$ shows a peak close to the pivot point. Inside the pivot point, the inward rapid propagations of $\hat{\mathcal{N}}$ and $\hat{\mathcal{S}}$ are observed. This issue of the inward propagation is discussed in the last part of the Letter.

The picture of the LCO is that of oscillations which occur in the density gradient (narrow barrier), localized edge radial electric field, and turbulence intensity, in the region of -2 cm $< r - a < 0$ cm. The causal relation among them is depicted by a Lissajous diagram. The conditional average for the LCO phase in D_α is used to obtain an averaged time evolution for one period. The Lissajous diagram $(\hat{E}_r, \hat{\mathcal{S}})$ is displayed in Fig. 3(a) for signals at three locations where the $\hat{E}_r$ has high coherence with $\hat{D}_\alpha$. The Lissajous diagram $(\hat{E}_r, -\hat{L}_n^{-1})$, where $L_n^{-1} \equiv -\nabla n/n \sim -\nabla I_{\mathrm{HIBP}}/\bar{I}_{\mathrm{HIBP}}$ is the inverse density gradient scale length, is shown in Fig. 3(b). The relative changes in the LCO of $L_n^{-1} \propto \nabla n$, E_r, and $\mathcal{S}$ amount to 25%, 50%, and 25%, respectively, at $r - a \sim -1$ cm. For the two locations near the pivot point ($r - a \sim -0.8 - 1.4$ cm), E_r remains negative, and the Lissajous diagram $(\hat{E}_r, \hat{\mathcal{S}})$ shows a clockwise rotation. This indicates that the increase of $\hat{E}_r$ (or that of $|\hat{E}_r'|$) leads the reduction of turbulence, and the higher turbulence state corresponds to the reduction of $\hat{E}_r$ [20]. [At the outermost location $r - a \sim -0.2$ cm, the Lissajous diagram shows clockwise rotation.] The Lissajous diagram $(\hat{E}_r, -\hat{L}_n^{-1})$ shows that an increase of $-\hat{E}_r$ precedes that of $\hat{L}_n^{-1}$. The Lissajous curve $(\hat{L}_n^{-1}, \hat{\mathcal{S}})$ moves counterclockwise and gives an approximate phase relation as $\partial \hat{L}_n^{-1}/\partial t \propto \mathcal{S}_0 - \hat{\mathcal{S}}$ and $\partial \hat{\mathcal{S}}/\partial t \propto \hat{L}_n^{-1} - g_0$, where $\mathcal{S}_0$ and g_0 are phenomenological critical values. These observations indicate the link that the increase of $-\hat{E}_r$ leads to both decay of $\hat{\mathcal{S}}$ and growth of $\hat{L}_n^{-1}$. The increased $\hat{L}_n^{-1}$ tends to accelerate increments of $-\hat{E}_r$ but causes the growth of $\hat{\mathcal{S}}$, which finally closes the loop of the LCO. This LCO dynamics occurs in the region of

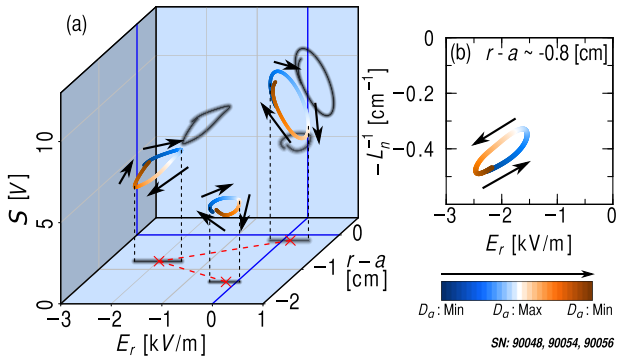

FIG. 3 (color online). (a) Lissajous diagram between E_r and $\mathcal{S}$ at the LCO frequency for various radii. The profile of mean E_r is also shown by a dashed red line. (b) Lissajous diagram between E_r and L_n^{-1} at the LCO frequency for the location close to the pivot point. Color bar shows the phase of the LCO in D_α, where dark blue and orange correspond to the minimum of D_α, and white means the maximum of D_α. Arrows show their rotating direction.

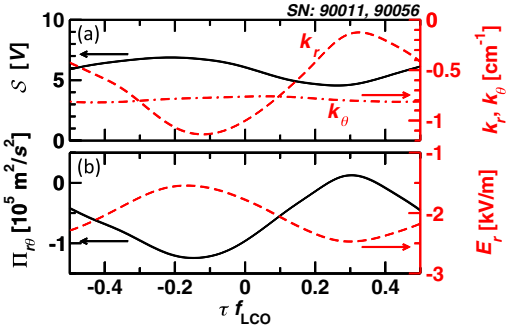

FIG. 4 (color online). Conditional averaged time evolutions of (a) $\mathcal{S}$, k_r and k_θ, (b) $\Pi_{r\theta}$ and E_r. The phase of the D_α LCO is used for the horizontal axis (the origin corresponds to the peak of D_α).

parameters $\rho_p L_n^{-1} \sim 0.7$ which is close to the critical condition of bifurcation [5]. These features semiquantitatively agree with the model in Ref. [5] and do not include the zonal flows.

We have also evaluated the turbulent Reynolds stress and found that it has only a small role in generating the oscillatory $E \times B$ velocity in the LCO. The turbulent Reynolds stress per unit mass density is given as $\Pi_{r\theta} = \langle \tilde{E}_r \tilde{E}_\theta \rangle / B^2 = -\mathcal{S}^2 k_r k_\theta / 2B^2$. Figures 4(a) and 4(b) show the waveforms of $\mathcal{S}$, k_r and k_θ, $\Pi_{r\theta}$, and E_r, respectively, which are obtained by a conditional average of 21 oscillation periods at $r - a \sim -1$ cm. Modulation amplitudes of $\hat{\Pi}_{r\theta}$ are evaluated as $|\hat{\Pi}_{r\theta}| \sim 0.7 \times 10^5$ m^2/s^2. The force in the poloidal direction per unit mass is $\partial \hat{\Pi}_{r\theta}/\partial r$, the magnitude of which is evaluated as $|\hat{\Pi}_{r\theta}| L^{-1}$. ($L \sim 1$ cm denotes the scale length of the radial gradient of $\hat{\Pi}_{r\theta}$.) The equation for the evolution of $E \times B$ velocity takes a form $\epsilon_\perp \partial \hat{V}_{E\times B}/\partial t = \partial \hat{\Pi}_{r\theta}/\partial r + \cdots$, where the ellipsis indicates additional effects, like the collisional damping term [21,22]. Here, the coefficient $\epsilon_\perp$ denotes the relative dielectric constant for a radial electric field (the ratio between the dielectric constant to that of vacuum ϵ_0). The collisionality in the plasma edge is in the plateau regime (normalized ion collisionality $\nu_{*,i}$ is $\sim$2.6), so that $\epsilon_\perp$ was given as $1 + 2q^2$ [21]. From this equation of motion, the oscillatory velocity, which is induced by the oscillatory Reynolds stress at the angular frequency of $\omega_{\rm LCO} = 2\pi f_{\rm LCO}$, is evaluated as $\delta|\hat{V}_{E\times B}| \sim |\hat{\Pi}_{r\theta}| L^{-1} \epsilon_\perp^{-1} \omega_{\rm LCO}^{-1}$. By use of parameters $|\hat{\Pi}_{r\theta}| L^{-1} \sim 7 \times 10^6$ m/s^2, $\omega_{\rm LCO} \sim 3 \times 10^4$ s^{-1}, and $\epsilon_\perp \sim 20$ for $q \sim 3$, one has the amplitude of modulation $\delta|\hat{V}_{E\times B}| \sim 15$ m/s. The contribution is much smaller than the modulation of $E \times B$ velocity in the LCO (~ 500 m/s). This small role of turbulence in poloidal acceleration is consistent with the observation that the oscillatory flow in LCO is not zonal flows.

Figure 2(g) shows that $\hat{\mathcal{N}}$ propagates inward with the wave number of propagation Re $k_r = 25 \pm 2$ m^{-1} (for $r - a < -1.5$ cm). The propagation velocity is given as $\omega_{\rm LCO}/{\rm Re}\ k_r \sim 900$ m/s, which is of the order of the diamagnetic velocity (inside the pivot point radius). Here, the rapid propagation of $\hat{\mathcal{N}}$ is compared to two different models: the ballistic propagation model and the diffusion model. Figures 2(g) and 2(h) indicate that the phase of $\mathcal{N}$ precedes that of $\mathcal{S}$ by the amount of $\sim 0.7\pi$. That is, the phase of $-\nabla n$ leads that of $\mathcal{S}$ by $\sim 0.2\pi$, or the $-\nabla n$ oscillation propagates inward, leading to $\mathcal{S}$ oscillation. These results of the propagation velocity and phase relation are consistent with theories of ballistic propagation [23–26]. If one interprets the observation in terms of the diffusion model, the effective diffusivity (defined by $\hat{\Gamma} = -D_{\rm eff} \partial \hat{n}/\partial r$) is fitted to $D_{\rm eff} = \omega_{\rm LCO}/2({\rm Re}\, k_r)^2 \sim 23$ m^2/s, which is much larger than the transport coefficient deduced in the stationary state [27]. The penetration of these modulations up to the order of 10 cm has been observed. This phenomenon of propagation might be related to the fast core-edge coupling problem after the H-mode transition.

We note that we employ here two criteria for zonal flows, that they have substantial radial wave number k_r, and that they are primarily driven by turbulence Reynolds stress [6]. Except that ASDEX-U has confirmed GAMs from the frequency [10], the identification of low frequency zonal flows has not been completed in literature. In Ref. [11], which stated zonal flows, k_r has not been fully addressed. The study of the relative dielectric constant $\epsilon_\perp$ has not been completed in DIII-D and EAST [11,13]. In the LCO of JFT-2M, k_r of the perturbed potential is very small and the turbulence Reynolds stress is too small to explain the oscillatory flow. Thus, we conclude that zonal flows do not exist in the LCO, as is discussed in this article.

We thank P. H. Diamond, G. R. Tynan, U. Stroth, J.-Q. Dong, K. J. Zhao, C. Hidalgo, S. Sugita, and M. Sasaki for useful discussions, and the late H. Maeda, Y. Hamada, M. Mori, and Y. Kamada for strong support. One of the authors (T. K.) acknowledges M. Lesur for his help. This work is partly supported by the Grant-in-Aid for Scientific Research of JSPF, Japan (21224014, 23244113), the Grant-in-Aid for JSPS Fellows (24-7632), the collaboration programs of JAEA and of the RIAM of Kyushu University, and the Asada Science Foundation.

*Corresponding author.
kobayashi@riam.kyushu-u.ac.jp

[1] F. Wagner *et al.*, Phys. Rev. Lett. **49**, 1408 (1982).
[2] S.-I. Itoh and K. Itoh, Phys. Rev. Lett. **60**, 2276 (1988).
[3] H. Biglari, P. H. Diamond, and P. W. Terry, Phys. Fluids B **2**, 1 (1990).
[4] ASDEX Team, Nucl. Fusion **29**, 1959 (1989); see pp.1969–1973.
[5] S.-I. Itoh, K. Itoh, A. Fukuyama, Y. Miura, and the JFT-2M Group, Phys. Rev. Lett. **67**, 2485 (1991).

[6] P. H. Diamond, S.-I. Itoh, K. Itoh, and T. S. Hahm, Plasma Phys. Controlled Fusion **47**, R35 (2005).
[7] E.-j. Kim and P. H. Diamond, Phys. Rev. Lett. **90**, 185006 (2003).
[8] T. Estrada, T. Happel, C. Hidalgo, E. Ascasíbar, and E. Blanco, Europhys. Lett. **92**, 35 001 (2010).
[9] S. J. Zweben, R. J. Maqueda, R. Hager, K. Hallatschek, S. M. Kaye, T. Munsat, F. M. Poli, A. L. Roquemore, Y. Sechrest, and D. P. Stotler, Phys. Plasmas **17**, 102502 (2010).
[10] G. D. Conway, C. Angioni, F. Ryter, P. Sauter, and J. Vicente, Phys. Rev. Lett. **106**, 065001 (2011).
[11] G. S. Xu *et al.*, Phys. Rev. Lett. **107**, 125001 (2011).
[12] M. Xu, G. R. Tynan, P. H. Diamond, C. Holland, J. H. Yu, and Z. Yan, Phys. Rev. Lett. **107**, 055003 (2011).
[13] L. Schmitz, L. Zeng, T. L. Rhodes, J. C. Hillesheim, E. J. Doyle, R. J. Groebner, W. A. Peebles, K. H. Burrell, and G. Wang, Phys. Rev. Lett. **108**, 155002 (2012).
[14] G. R. Hill *et al.*, *Proceedings of the IAEA Fusion Energy Conference, OV/1–1, 2012* (IAEA, Vienna, 2012).
[15] G. R. Tynan *et al.*, *Proceedings of the IAEA Fusion Energy Conference, EX/10–3, 2012* (IAEA, Vienna, 2012).
[16] T. Ido *et al.*, Plasma Phys. Controlled Fusion **48**, S41 (2006).
[17] J. G. Cordey, D. G. Muir, S. V. Neudachin, V. V. Parail, E. Springmann, and A. Taroni, Nucl. Fusion **35**, 101 (1995).
[18] T. Ido *et al.*, Nucl. Fusion **46**, 512 (2006).
[19] K. Ida, and S. Hidekuma, Phys. Rev. Lett. **65**, 1364 (1990).
[20] J. Cheng *et al.*, Phys. Rev. Lett. **110**, 265002 (2013); after completing this Letter, we were informed that a similar directionality of limit cycle between E_r and $\mathcal{S}$ was reported on the HL-2A tokamak.
[21] K. Itoh and S.-I. Itoh, Plasma Phys. Controlled Fusion **38**, 1 (1996).
[22] M. N. Rosenbluth and F. L. Hinton, Phys. Rev. Lett. **80**, 724 (1998).
[23] X. Garbet, Y. Sarazin, F. Imbeaux, P. Ghendrih, C. Bourdelle, O. D. Gurcan, and P. H. Diamond, Phys. Plasmas **14**, 122305 (2007).
[24] S. Sugita, K. Itoh, S.-I. Itoh, M. Yagi, G. Fuhr, P. Beyer, and S. Benkadda, Plasma Phys. Controlled Fusion **54**, 125001 (2012).
[25] T. S. Hahm, P. H. Diamond, Z. Lin, K. Itoh, and S.-I. Itoh, Plasma Phys. Controlled Fusion **46**, A323 (2004).
[26] Ö. D. Gürcan, P. H. Diamond, T. S. Hahm, and Z. Lin, Phys. Plasmas **12**, 032303 (2005).
[27] T. Yamauchi, T. Shoji, and S. Yamamoto, Plasma Phys. Controlled Fusion **30**, 133 (1988).